MODELING OF DROP VAPORIZATION AND COMBUSTION WITH REGARD FOR SPRAY EFFECTS

S. M. Frolov, V. Ya. Basevich, A. A. Belyaev, V. S. Posvyanskii, and V. A. Smetanyuk

A mathematical model for drop vaporization, ignition, and combustion in a spatially uniform monodisperse drop suspension is proposed and applied for numerical studies of spray effects.

1 INTRODUCTION

Drop combustion is a phenomenon comprising all main constituents of the combustion process, namely, fast exothermic chemical reactions complicated by diffusion of reactants and products, thermal energy deposition, spreading of heat in the medium, and convective flows. The classical theory implies that drop combustion is diffusion limited and therefore chemical kinetic aspects are out of the analysis [1–4]. In addition, the classical theory considers an isolated drop in unconfined ambience. Within these presumptions, notable progress in understanding relevant physical and chemical processes has been achieved recently [5–8]. However, for problems dealing with combustion-generated pollutants and transient modes of combustion, like ignition or extinction, it is necessary to consider the effects of finite-rate chemical kinetics. Moreover, in practice, drop vaporization, ignition, and combustion occur in presence of neighboring drops or confinement surfaces. The corresponding effects are usually referred to as 'spray' and 'confinement' effects. Spray effects manifest themselves in two-phase reactive flows [9–15]. In existing computational approaches, chemical reaction rates are determined based on considering gas-phase combustion with fuel drops treated as distributed source terms for fuel vapor. As a matter of fact, spray combustion is a complex combination of diffusion-controlled flames around individual drops, groups of drops, and gas-phase partially premixed flames.

The objective of this paper is to study drop vaporization, ignition, and combustion with extended kinetics of fuel oxidation and pollutant (CO, NO, and soot) formation, transient heating, and multicomponent diffusion, as well as spray effects taken into account.

2 FORMULATION

For a spatially uniform and monodisperse drop suspension in air, an elementary cell in the form of hexahedron (in the two-dimensional plane, see Figs. 1*a* and 1*b*) or polyhedron with faces in the form of equilateral triangles (in the three-dimensional (3D) space, see Fig. 1*c*) can be constructed around each drop [16].

The length of a polyhedron edge is equal to a half-distance between drops in suspension, R_c. Due to symmetry considerations, mass, momentum, and energy fluxes through the faces will be zero. Polyhedron volume, V_s, and surface area, S_c, are:

$$V_c = \frac{5\sqrt{2}}{3} R_c^3 , \quad S_c = 5\sqrt{3} R_c^2$$

Thus, drop behavior in the suspension can be modeled by solving the governing conservation equations for a single drop with symmetry boundary conditions at the polyhedron faces. As shown in [16] based on 3D simulation of laminar flow pattern around an evaporating drop, the polyhedron cell can be approximated with an elementary sphere. In this case, the 3D problem is reduced to one-dimensional formulation with zero-flux boundary conditions at the surface of the elementary sphere of radius R equal to:

$$R = \left(\frac{5\sqrt{2}}{4\pi} \right)^{1/3} R_c \approx 0.826 R_c$$

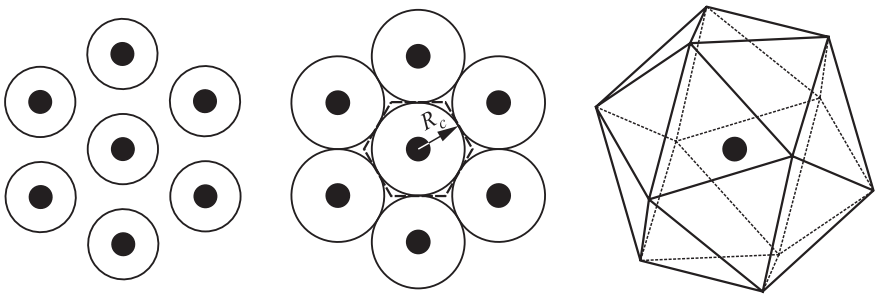

Figure 1 Elementary cell for the uniform monodisperse drop suspension. Black circles denote drops. Circumferences around drops characterize the spread of diffusion fluxes from individual drops. (*a*) Spray effects are absent; (*b*) spray effects manifest themselves. Dashed line bounds the elementary cell with zero mass and energy fluxes through its surface; R_c is the characteristic cell size (half-distance between drops); and (*c*) 3D elementary cell in the form of a regular polyhedron with 20 faces

The volume of the elementary sphere is $V = V_c$ and the surface area is $S/S_c \approx 0.99$. The error of such an approximation depends on the suspension density characterized by the loading ratio η — the mass of dispersed liquid in the unit volume. At a given loading ration, the radius of the elementary sphere is equal to:

$$R \approx R_0 \left(\frac{\rho_l}{\eta} \right)^{1/3}$$

where R_0 is the initial drop radius and ρ_l is the liquid density. In terms of the equivalence ratio, $\Phi = \eta/(\phi_{\rm st}\rho_g)$, the radius of the elementary sphere is equal to:

$$R \approx R_0 \left(\frac{\rho_l}{\rho_g \Phi \phi_{\rm st}} \right)^{1/3}$$

where ρ_g is the initial gas density and $\phi_{\rm st}$ is the stoichiometric fuel–air ratio. At normal atmospheric conditions, for stoichiometric mixtures of liquid hydrocarbon fuels, $\rho_g = 1.19$ kg/m^3, $\rho_l = 700$–800 kg/m^3, $\phi_{\rm st} \approx 0.06$, and $\Phi = 1$; therefore $\eta = \eta_{\rm st} \approx 0.07$–$0.08$ kg/m^3, $R_c/R_0 \approx 25$–27, and $R/R_0 \approx 21$–22. At elevated pressure, for example, at the end of compression stroke in a Diesel engine ($\rho_g \approx 30$ kg/m^3), $R_c/R_0 \approx 9$ and $R/R_0 \approx 8$.

The mathematical statement of the problem is described in detail in [16–18]. It is based on the following simplifying assumptions: (1) the drop has a spherical shape; (2) no internal diffusion of species and convection exist inside the drop; (3) buoyancy effects in a gas phase are not considered; (4) pressure is constant; and (5) concentration of fuel vapor at the drop surface is governed by the equilibrium relationship. The governing equations of the model include the partial differential equations of energy conservation in the drop; gas-phase continuity and energy conservation equations; multicomponent diffusion equations for gas-phase species, and the real-gas equation of state for the gas phase. All relevant physical processes are considered as functions of pressure and temperature.

Boundary conditions comprise the symmetry condition in the drop center; temperature, heat, and mass-flux continuity conditions at the drop surface; and the no-gradient conditions at the spherical elementary cell surface. As the model implies constant pressure, the radius of the elementary sphere is dependent of time, i.e., $R = R(t)$. The expansion/shrinking of the sphere is found from the solution by allowing the external boundary of the sphere to move with the local gas velocity at a radial distance $r = R$.

Initial conditions encounter homogeneous conditions inside and outside the drop. To facilitate drop ignition, a provision for a thin hot layer is made in the gas phase. The ambient temperature is taken equal or higher than the drop temperature. Initial fuel vapor content in the gas phase is taken either zero (in case of no prevaporization) or equal to a specified value depending on the drop prevaporization degree.

Gas-phase oxidation of a heavy hydrocarbon fuel is modeled by means of the overall reaction mechanism containing 10 species (fuel, O_2, N_2, CO, CO_2, H_2, H_2O, NO, soot (denoted as C), and a generalized radical $\mathcal{R}$). The mechanism is presented in Table 1. The values of corresponding Arrhenius and thermodynamic parameters are presented for n-heptane and n-tetradecane that are used below in calculations. In the mechanism of Table 1, the main chemical process responsible for heat release and taking into account dissociation and chain branching is represented by reactions Nos. 1 to 6. Reactions Nos. 7 to 10 describe formation and consumption of nitrogen oxide and soot. In general, the overall mechanism of Table 1 includes dependence of preexponential factors of some reactions on a local fuel–air ratio. However, herein this dependence is neglected. The kinetic mechanism has been preliminarily validated for propagating premixed flames, nonpremixed counterflow flames, fuel drop autoignition, and diffusion flames [19–23].

A set of governing equations was integrated numerically with the use of a nonconservative implicit finite-difference scheme and a movable, adapted, computational grid. The solution procedure included iterations at each time step. The important point of the algorithm is the linearization of the conditions at the drop interface. For ensuring rapid convergence of the iterations, the full Newton-type linearization of the interface conditions was required. The accuracy of the solution was controlled by checking the elementary balances of C and H atoms as well as the energy balance at each time step.

3 RESULTS AND DISCUSSIONS

Numerical solution of mass, momentum, and energy conservation equations for a hydrocarbon drop within the elementary sphere resulted in several important findings. Below these findings are discussed on examples of drop vaporization, autoignition, and combustion.

3.1 Drop Vaporization

The mathematical model has been validated against available experimental data on isolated drop vaporization [17, 18]. Figure 2 shows the comparison of predicted and measured [24] surface regression curves for a n-tetradecane drop of initial diameter $d_0 = 70$ μm evaporating in air at ambient temperature of $T_{g0} = 300$ °C.

Analysis of drop vaporization in dense drop suspensions indicates [16] that drop lifetime increases considerably as compared to an isolated drop in an unconfined atmosphere. Figure 3 shows the calculated time histories of the squared drop diameter depending on Φ. Three important findings are worth mentioning:

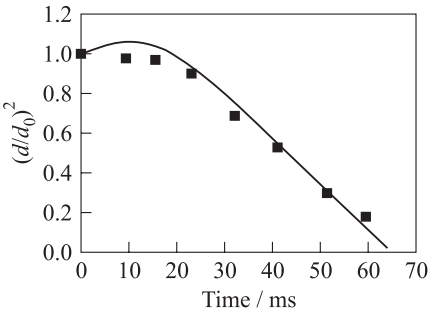

Figure 2 Comparison of the predicted $d^2(t)$-curve with experimental data [24] on evaporation of an unsupported n-tetradecane drop with $d_0 = 70 \pm 2$ μm in air at ambient temperature of $T_{g0} = 300$ °C

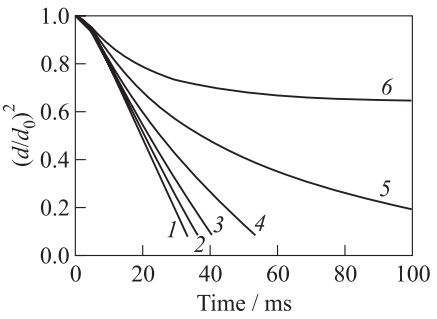

Figure 3 Predicted time histories of the normalized surface of an n-heptane drop evaporating in air as a function of Φ [16]. Initial parameters: drop diameter $d_0 = 70$ μm, drop temperature $T_{l0} = 293.15$ K, gas temperature $T_{g0} = 573.15$ K, and pressure $p = 0.1$ MPa. *1* — $\Phi = 0$ (isolated drop), *2* — 1.06, *3* — 2.12, *4* — 4.25, *5* — 8.5, and *6* — 17.0

(1) drops evaporate slower; (2) the deviations from the classical d^2-law increase as Φ increases; and (3) at a certain Φ, drops evaporate only partly. The latter finding is due to a considerable screening effect of neighboring drops in the cloud resulting in vapor saturation conditions in the interdrop space. Slower vaporization of individual drops has been observed in experiments with linear drop arrays [25].

3.2 Drop Autoignition

To validate the reaction mechanism of Table 1 for autoignition of isolated n-heptane drops, the predicted values of autoignition delay were compared to the experimental data obtained under microgravity conditions [26, 27]. The initial drop temperature was set to $T_{l0} = 293.15$ K. The ambient gas temperature around the drop was taken spatially homogeneous and equal to T_{g0}. Size of the computational domain around the drop, R_m, was taken sufficiently large as compared with the initial drop radius, r_0, so the parameters at the outer boundary of the computational domain were kept constant during computation.

After some time interval, referred to as the ignition delay, autoignition occurs at a certain distance from the drop surface. The autoignition delay is determined from the maximum temperature history as the time taken for the maximum

Table 2 Comparison of predicted and measured autoignition delay times for isolated n-heptane drops at pressure of 1 atm

Initial drop diameter, μm	Air temperature, K	Autoignition delay, s	
		measured	predicted
700	1000	0.30 [26]	0.19
1000	960	0.58 [27]	0.48

temperature increase rate to reach a preset value of $T'_{\max} = 10^6$ K/s. Other reasonable definitions of ignition delay were also tested (e.g., with $T'_{\max} = 10^7$ K/s, etc.). All definitions provided very similar results for the autoignition delay. The comparison between predicted and measured [26, 27] ignition delays for n-heptane drops is presented in Table 2.

Figures 4a and 4b show the predicted time histories of the maximal temperature around n-heptane (Fig. 4a) and n-tetradecane (Fig. 4b) drops at autoignition conditions (drop temperature $T_{l0} = 293.15$ K, gas temperature $T_{g0} = 1200$ K, and pressure $p = 0.1$ MPa). An isolated n-heptane drop does not ignite at these conditions, whereas n-tetradecane drop ignites (see curves *1*). Spray effects are illustrated by curves *2* to *4* corresponding to $\Phi = 0.5$, 1.0, and 2.0, respectively. For n-heptane drop suspension, the shortest ignition delay time is attained for the stoichiometric composition with $\Phi = 1.0$ (curve *3* in Fig. 4a). The fuel-rich suspension of n-heptane drops with $\Phi = 2.0$ ignites only when

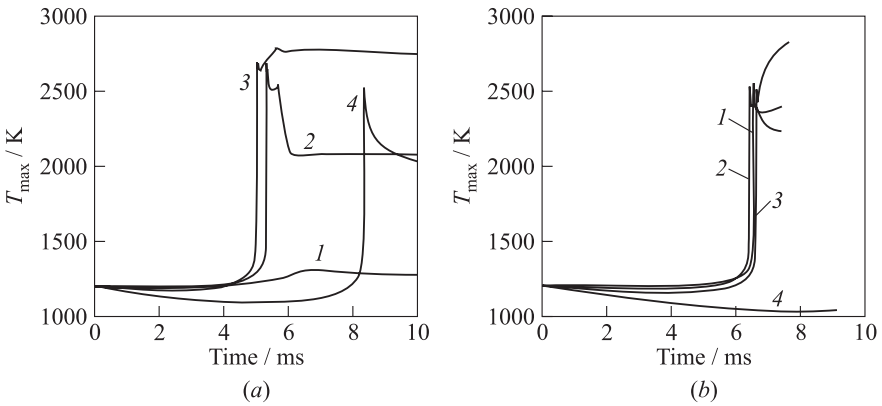

Figure 4 Predicted time histories of maximal temperature around n-heptane (a) and n-tetradecane (b) drops at autoignition conditions. Initial parameters: drop diameter $d_0 = 50$ μm, drop temperature $T_{l0} = 293.15$ K, gas temperature $T_{g0} = 1200$ K, and pressure $p = 0.1$ MPa. *1* — $\Phi = 0$ (isolated drop), *2* — 0.5, *3* — 1.0, and *4* — 2.0

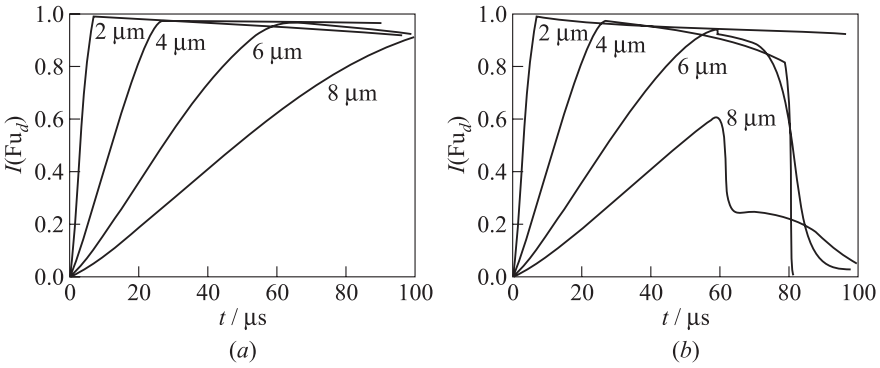

Figure 5 Predicted time histories of fuel index $I(\mathrm{Fu}_d)$ in a stoichiometric spray of small n-heptane drops with $d_0 = 2$, 4, 6, and 8 μm at initial air pressure and temperature of 3 MPa and 1500 K, respectively: (a) $\mathrm{Fu}_g = 0$, and (b) $\mathrm{Fu}_g = 0.25$

the drops are completely vaporized. For the n-tetradecane drop suspension, the shortest ignition delay time is attained for the fuel-lean composition with $\Phi = 0.5$ (curve 2 in Fig. 4b). The fuel-rich suspension of n-tetradecane drops with $\Phi = 2.0$ does not ignite, at least during 10 ms. Thus, autoignition behavior is very sensitive to the suspension density and fuel properties.

It is instructive to introduce a fuel index as the ratio of fuel mass in the gas phase to the initial drop mass:

$$I(\mathrm{Fu}) = \frac{6}{\pi d_0^3 \rho_l} \int_{r_s}^{R} 4\pi r^2 Y(t,r)\, dr \tag{1}$$

where Y is the partial fuel vapor density, r_s is the instantaneous drop radius, and Fu stands for fuel. There are two fuel indices: $I(\mathrm{Fu}_d)$ — for the fuel vapor originating from the drop due to its vaporization at time $t > 0$, and $I(\mathrm{Fu}_g)$ — for the fuel vapor existing in the gas phase at $t = 0$ due to drop prevaporization.

Figures 5a and 5b show the time histories of fuel index $I(\mathrm{Fu}_d)$ in a stoichiometric spray for small n-heptane drops from 2 to 8 μm in initial diameter with no prevaporization (a) and with $I(\mathrm{Fu}_g) = 0.25$. At the conditions adopted ($T_{g0} = 1500$ K and $p = 3$ MPa), drops of initial diameter 2 μm evaporate in approximately 5.8 μs; however, chemical reaction is almost absent during a period of 0.1 ms. The same is valid for drops 4, 6, and 8 μm in diameter. Combustion is considerably accelerated if at the beginning of the process, the gas phase contains some amount of prevaporized fuel. Note that the total initial equivalence ratio was always kept constant and equal to 1, i.e., in cases with $\mathrm{Fu}_g > 0$, the radius of the elementary sphere R was correspondingly changed.

It follows from Fig. 5*b* that during ignition delay period fuel vapor accumulates around the drop and after ignition it is rapidly consumed. Clearly, at $\mathrm{Fu}_g > 0$, the rate of $I(\mathrm{Fu}_d)$ decay can change drastically starting from a certain time. For example, at $t = 60$ μs, drops of initial diameter 6 μm exhibit fast decrease of fuel vapor concentration (see Fig. 5*b*) caused by ignition of initially prevaporized fuel. After ignition, the rate of fuel vapor depletion decreases due to transition to diffusion controlled drop combustion. At $t = 100$ μs, only 2.5% of fuel vapor remains unburned. In case of drops of initial diameter 8 μm, 4.6% of fuel vapor remains unburned at $t = 100$ μs. Suspensions with drops of initial diameter 4 μm ignite with the ignition delay of approximately 80 μs (strong cooling due to evaporation manifests itself), but completely burn out before 100 μs. Suspensions with drops of initial diameter 2 μm do not ignite during 100 μs. Thus, the ignition delay and fuel burning time in the spray are complex functions of the initial drop diameter and are strongly affected by the amount of prevaporized fuel.

3.3 Drop Combustion

The mathematical model was also validated against available experimental data for isolated drop combustion. A curve in Fig. 6 shows the predicted dependence of the combustion constant K of n-heptane drops on the initial drop diameter. In the calculations, the combustion constant is determined as the slope of the $d^2(t)$-curve at the quasi-steady period of drop combustion, i.e.,

$$K = -\frac{d(d_s^2)}{dt}$$

where $d_s = 2r_s$.

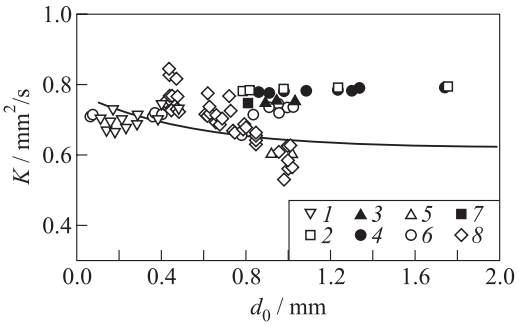

Figure 6 Comparison of predicted (curve) and measured (symbols) dependencies of n-heptane combustion constant K on the initial drop diameter at normal pressure. Experimental data: *1* — [28], *2* — [29], *3* — [30], *4*, *5* — [31], *6* — [32], *7* — [33], *8* — [34]

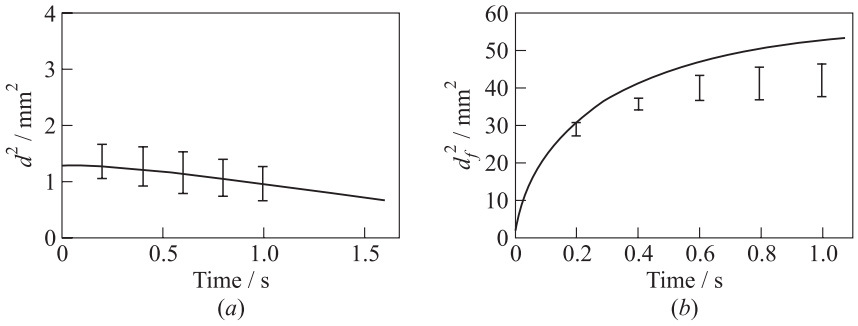

Figure 7 Comparison of predicted (curves) and measured (error bars) dependencies of drop (a) and flame (b) diameter for a burning n-decane drop under low-gravity conditions at normal pressure. Experimental data [35]

Symbols in Fig. 6 represent experimental data [28–34] obtained both under microgravity conditions and normal gravity conditions. In some experimental studies (e.g., [28]) the combustion constant was defined as $K = d_0^2/t_d$, where t_d is the drop burning time. Clearly, the model correlates fairly well with the measurements for drops of relatively small initial size. For drops of large initial diameter, the combustion constant is somewhat underpredicted. Note that for such drops, the contribution of convective heat and mass transfer becomes significant, while the model does not include these effects.

For n-decane drops, the model provides satisfactory agreement with low-gravity experimental data [35] for the evolution of drop (Fig. 7a) and flame (Fig. 7b) diameter.

In the above examples, the maximum gas temperature attained during the drop lifetime varies from 1800 to 2200 K, with higher temperature values related to initially larger drops.

The predicted dynamics and structure of the drop flame exhibits several important features. The first one is the existence of a soot shell located between the flame and the drop surface. The second is that the flame, after drop ignition, moves outwards from the droplet, but at later stages, it changes the direction of motion (flame "shrinks"). These both features were observed experimentally [31, 35–38], and reviewed in [39].

Figure 8 shows the predicted histories of the drop radius r_s, flame radius r_f (determined as the radial position of temperature maximum), and soot shell radius r_{soot} (determined as the radial position of maximum soot concentration). When considering Fig. 8, one can distinguish three stages in the drop history: (1) ignition, (2) outward flame motion, and (3) flame "shrinking." The burning process of a drop is accompanied with the formation of a spherical soot

shell inside the flame. The mass fraction of soot in this shell structure remains nearly constant as combustion proceeds until near the end of burning when the flame begins to "shrink." The "shrinking" flame approaches the soot shell, resulting in soot oxidation before flame extinguishing. This understanding of soot formation mechanism at drop combustion provides the measures to control soot emission, for example, by applying water-in-oil emulsions [40].

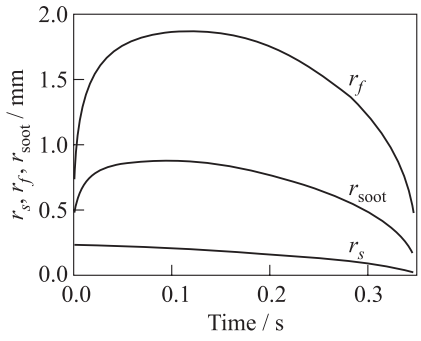

Figure 8 Predicted histories of drop radius, r_s, flame radius, r_f, and soot shell radius, r_{soot}, during ignition and combustion of n-heptane drop of initial diameter 0.48 mm in air at ambient pressure of 0.1 MPa and temperature of 300 K

Similar to vaporization, volumetric combustion in dense drop suspensions is very sensitive to the drop loading ratio. The lifetime of burning drops also increases with Φ. Moreover, temperature and flame dynamics in the interdrop space behave very different from that typical for the isolated drop other conditions being equal. Figure 9 shows the calculated time histories of the flame (maximum) temperature $T_{\max}$ as well as dimensionless flame and drop radii, r_f/r_0 and r_s/r_0, respectively, for the iso-

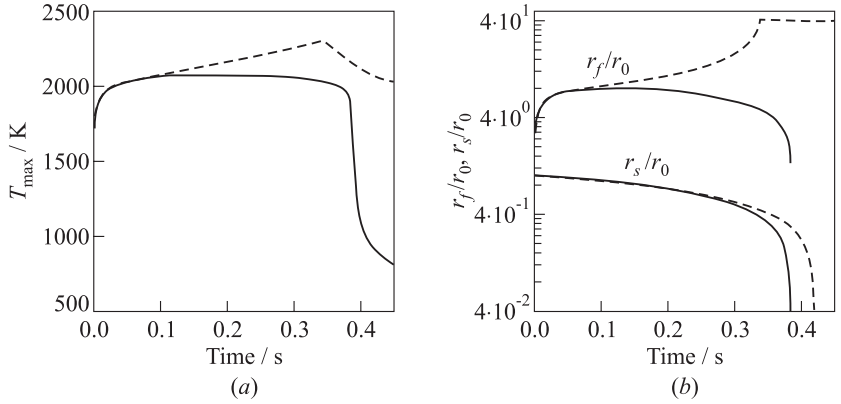

Figure 9 Comparison of flame temperature (a) and dimensionless flame and drop radii, r_f/r_0 and r_s/r_0, histories (b) for the isolated drop (solid curve) and drop in suspension (dashed curves, $\Phi = 1.1$). Fuel: n-heptane. Oxidizer: air. Initial pressure and temperature: 0.1 MPa and 300 K; $r_0 = 0.25$ mm

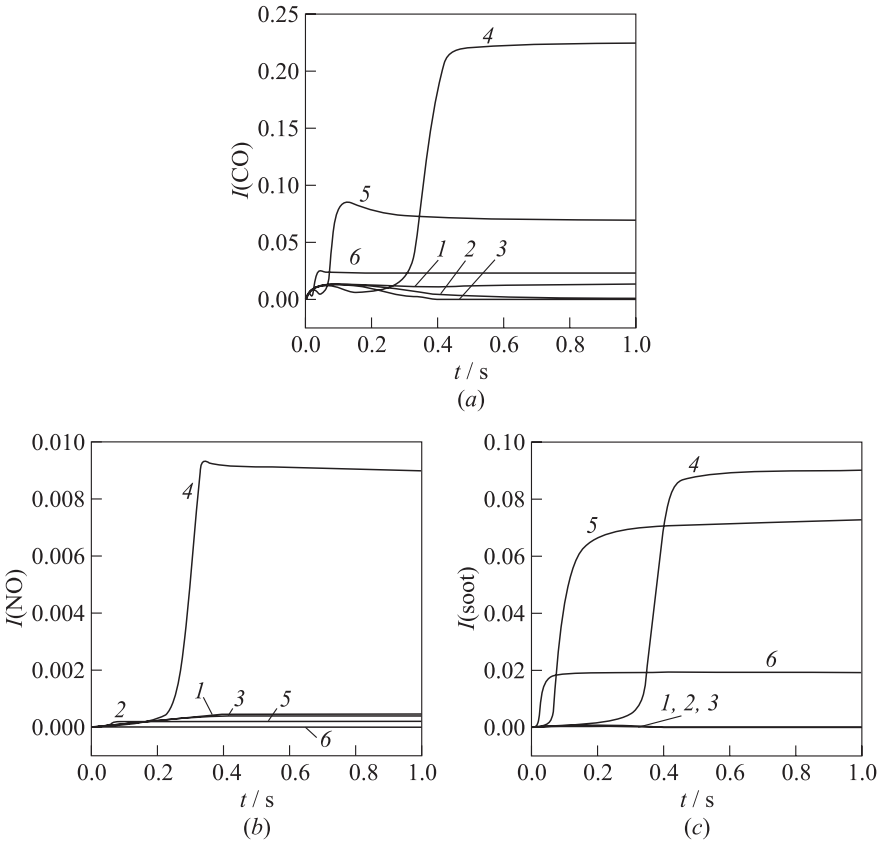

Figure 10 Predicted time histories of emission indices of CO (*a*), NO (*b*), and soot (*c*) for burning drops in suspension depending on Φ. Initial parameters: $d_0 = 0.5$ mm, $T_{l0} = T_{g0} = 293.15$ K, and $p = 0.1$ MPa. *1* — $\Phi = 0$ (isolated drop), *2* — 0.32, *3* — 0.55, *4* — 1.1, *5* — 5.3, and *6* — $\Phi = 18.5$

lated drop (solid curves) and drop in suspension (dashed curves) of similar initial radius $r_0 = d_0/2 = 0.25$ mm.

The suspension density in this case is characterized by the equivalence ratio $\Phi = 1.1$. The flame temperature for the drop in suspension is considerably higher than that for the isolated drop; in particular, at the end of combustion. For the isolated drop, the flame stabilizes at a distance of about $8r_0$, whereas for the drop in suspension, the flame spreads towards the edge of the elementary sphere consuming all available oxygen. In fuel-rich suspensions, only a part of fuel is burned and the remaining fuel is vaporized and accumulated in the interdrop space together with the combustion products. As the temperature in

the interdrop space is high, fuel vapor can partly decompose to more reactive intermediate species.

Emission indices of pollutants depend considerably on the suspension density. Figure 10 shows the predicted emission indices of CO (a), NO (b), and soot (c). The emission indices are defined by Eq. (1) with Y treated as the partial density of the corresponding species in the gas phase. It follows from Fig. 10 that the near-stoichiometric suspensions exhibit maximal emission indices. As could be expected, fuel-rich suspensions exhibit higher emission indices of CO and soot, but lower emission indices of NO than the fuel-lean mixtures.

4 CONCLUDING REMARKS

Based on the detailed simulation of drop behavior in a uniform monodisperse suspension, it has been shown that (1) drops in suspension vaporize slower than isolated drops; (2) quasi-stationary d^2-law is, in general, not valid for drops in suspension; (3) at suspension densities exceeding a certain limiting value, drops vaporize only partly or virtually do not vaporize; (4) drop autoignition delay depends on the drop diameter and suspension density and is strongly affected by the amount of prevaporized fuel; (5) individual drop flame structure and parameters depend on the suspension density; (6) individual drop flame exists within a limited range of suspension densities; and (7) emission indices of pollutants (CO, NO, and soot) depend considerably on the suspension density. Results of calculations have been compared with available experimental data. The analysis reported herein is also applicable for approximate description of local phenomena in nonuniform polydisperse drop suspensions. It is intended to use the results for improved ignition and combustion modeling in two-phase reactive flows.

ACKNOWLEDGMENTS

This work was supported by the Russian Foundation for Basic Research (grants No. 02-03-33168) and International Science and Technology Center (project 2740).

REFERENCES

1. Varshavskii, G. A. 1945. In: *Trans. of NII-1* 6.
2. Godsave, G. A. E. 1953. Studies of the combustion of drops in a fuel spray — the burning of single drops of fuel. *4th Symposium (International) on Combustion Proceedings*. Baltimore, MD: Williams and Wilkins Co. 818–30.

3. Spalding, D. B. 1953. The combustion of liquid fuels. *4th Symposium (International) on Combustion Proceedings*. Baltimore, MD: Williams and Wilkins Co. 847–64.
4. Goldsmith, M., and S. S. Penner. 1954. On the burning of single drops of fuel in an oxidizing atmosphere. *Jet Propulsion* 24(4):245–51.
5. Law, C. K. 1982. Recent advances in droplet vaporization and combustion. *Progress Energy Combustion Sci.* 8:171–201.
6. Sirignano, W. A. 1983. Fuel droplet vaporization and spray combustion theory. *Progress Energy Combustion Sci.* 9:291–322.
7. Bachalo, W. D. 1995. A review of laser scattering in spray. *25th Symposium (International) on Combustion Proceedings*. Pittsburgh, PA: The Combustion Institute. 333.
8. Mashayek, F., and R. V. R. Pandya. 2003. Analytical description of particle/ droplet-laden turbulent flows. *Progress Energy Combustion Sci.* 29:329.
9. Twardus, E. M., and T. A. Brzustowski. 1977. The interaction between two burning fuel droplets. *Archiwum Processov Spalania*. 8:347.
10. Chiu, H. H., and T. M. Liu. 1977. Group combustion of liquid droplets. *Combustion Science Technology* 17:127.
11. Correa, S. M., and M. Sichel. 1983. The group combustion of a spherical cloud of monodisperse fuel droplets. *19th Symposium (International) on Combustion Proceedings*. Pittsburgh, PA: The Combustion Institute.
12. Marberry, M., A. K. Ray, and K. Leung. 1984. Effect of multiple particle interactions on burning droplets. *Combustion Flame* 57:237.
13. Nigmatulin, R. I. 1987. *Dynamics of multiphase media*. Part 1. Moscow: Nauka Publ.
14. Dwyer, H. A., H. Nirschl, P. Kerschl, and V. Denk. 1994. Heat, mass, and momentum transfer about arbitrary groups of particles. *25th Symposium (International) on Combustion Proceedings*. Pittsburgh, PA: The Combustion Institute. 389.
15. Sivasankaran, K., K. N. Seetharamu, and R. Natarajan. 1996. Numerical investigation of the interference effects between two burning fuel spheres. *Int. J. Heat Mass Transfer* 39:3949.
16. Frolov, S. M., V. Ya. Basevich, V. S. Posvianskii, and V. A. Smetanyuk. 2004. Vaporization and combustion of hydrocarbon fuel drop. Part IV. Drop vaporization with regard for spray effects. *Rus. J. Chemical Physics* 23(7):49–58.
17. Basevich, V. Ya., A. A. Belyaev, A. V. Evlampiev, V. S. Posvyanskii, and S. M. Frolov. 2002. Vaporization and combustion of hydrocarbon fuel drop. Part I. Nonempirical model of single-component drop vaporization. *Rus. J. Chemical Physics* 21(3):58–67.
18. Frolov, S. M., V. S. Posvianskii, V. Ya. Basevich, A. A. Belyaev, V. A. Smetanyuk, V. V. Markov, and I. V. Semenov. 2004. Vaporization and combustion of hydrocarbon fuel drop. Part II. Nonempirical model of drop vaporization with regard for multicomponent diffusion. *Rus. J. Chemical Physics* 23(4):75–83.
19. Basevich, V. Ya., A. A. Belyaev, and S. M. Frolov. 1998. Overall kinetic mechanisms of laminar flames for modeling turbulent reactive flows. I. Main chemical process of energy deposition. *Rus. J. Chemical Physics* 17(9):112.

20. Basevich, V. Ya., A. A. Belyaev, and S. M. Frolov. 2001. Modeling of two-phase turbulent combustion based on the equivalent flame concept. *Rus. J. Chemical Physics* 20(12):37.

21. Evlampiev, A. V., S. M. Frolov, V. Ya. Basevich, and A. A. Belyaev. 2001. Overall kinetic mechanisms for modeling turbulent reactive flows. IV. Nonpremixed combustion. *Chemical Physics Reports* 20(11):21–27.

22. Frolov, S. M., V. Ya. Basevich, A. A. Belyaev, V. S. Posvianskii, and V. A. Smetanyuk. 2003. Detailed modeling of drop evaporation and combustion. In: *Combustion and atmospheric pollution*. Eds. G. D. Roy, S. M. Frolov, and A. M. Starik. Moscow: TORUS PRESS. 207–13.

23. Frolov, S. M., V. Ya. Basevich, and V. S. Posvyanskii. 2004. Limiting drop size and prevaporization degree required for spray detonation. In: *Application of detonation to propulsion*. Eds. G. Roy, S. Frolov, and J. Shepherd. Moscow: TORUS PRESS. 110–19.

24. Massoli, P., M. Lazarro, F. Beretta, and A. D'Alessio. 1993. Characterization of hydrocarbon droplets heating in a drop tube furnace. Instituto Motori C.N.R. Rept. Research Activities and Facilities. Ed. A. D. Lorenzo. Napoli. 36–37.

25. Atthasit, A., N. Doue, Y. Biscos, G. Lavergne, and A. Berlemont. 2003. Influence of drop cocentration on the dynamics and evaporation of a monodisperse stream of drops in evaporation regime. In: *Combustion and atmospheric pollution*. Eds. G. D. Roy, S. M. Frolov, and A. M. Starik. Moscow: TORUS PRESS. 214–19.

26. Takei, M., H. Kobayashi, and T. Niioka. 1993. Ignition experiment of a blended fuel droplet in a microgravity field. *Int. J. Microgravity Res. Appl. Microgravity Sci. Technol.* VI/3:184–87.

27. Niioka, T., H. Kobayashi, and D. Mito. 1994. Ignition experiment on droplet array in normal and microgravity environments. *IVTAM Symposium Mechanics and Combustion of Droplet and Sprays Proceedings*. Tainan. 367–77.

28. Monaghan, M. T., R. G. Siddall, and M. W. Thring. 1968. The influence of initial diameter on the combustion of single drops of liquid fuel. *Combustion Flame* 12:45–53.

29. Kumagai, S., T. Sakai, and S. Okajima. 1971. Combustion of free fuel droplets in a freely falling chamber. *13th Symposium (International) on Combustion Proceedings*. Pittsburgh, PA: The Combustion Institute. 779–85.

30. Okajima, S., and S. Kumagai. 1975. Further investigations of combustion of free droplets in a freely falling chamber including moving droplets. *15th Symposium (International) on Combustion Proceedings*. Pittsburgh, PA: The Combustion Institute. 401–7.

31. Jackson, G.S., C. T. Avedisian, and J.C. Yang. 1992. Observations of soot during droplet combustion at low gravity: Heptane and heptane/monochloroalkane mixtures. *Int. J. Heat Mass Transfer* 35(8):2017–33.

32. Hara, H., and S. Kumagai. 1994. The effect of initial diameter on free droplet combustion with spherical flame. *25th Symposium (International) on Combustion Proceedings*. Pittsburgh, PA: The Combustion Institute. 423–30.

33. Mikami, M., H. Kato, J. Sato, and M. Kono. 1994. Interactive combustion of two droplets in microgravity. *25th Symposium (International) on Combustion Proceedings*. Pittsburgh, PA: The Combustion Institute. 431–38.

34. Jackson, G. S., and C. T. Avedisian. 1994. The effect of initial diameter in spherically symmetric droplet combustion of sooting fuels. *Proc. Royal Socyety London A* 446:255–76.

35. Shaw, B. D., F. L. Dryer, and F. A. Williams. 1988. Sooting and disruption in spherically symmetrical combustion of decane droplets in air. *Acta Astronautica* 17(11/12):1195–202.

36. Randolph, A. L., and C. K. Law. 1986. Influence of physical mechanisms on soot formation and destruction in droplet burning. *Combustion Flame* 64:267–84.

37. Avedisian, C. T., J. C. Yang, and C. H. Wang. 1988. On low-gravity droplet combustion. *Proc. Royal Society London A* 420:183–200.

38. Hara, H., and S. Kumagai. 1990. Experimental investigation of free droplet combustion under microgravity. *23rd Symposium (International) on Combustion Proceedings*. Pittsburgh, PA: The Combustion Institute. 1605–10.

39. Avedisian, C. T. 2000. Recent advances in soot formation from spherical droplet flames at atmospheric pressure. *J. Propulsion Power* 16(4):628–35.

40. Frolov, S. M., V. S. Posvyanskii, V. Ya. Basevich, A. A. Belyaev, O. Esmilaire, C. Jablon, and P. Schmelzle. 2001. Control of single droplet combustion and emission. *18th Colloquium (International) on Dynamics of Explosions and Reaction Systems*. Seattle, WA. Paper No. 142 (CD ROM).